Materials Research. 2019;22(6):e20190469
DOI: http://dx.doi.org/10.1590/1980-5373-MR-2019-0469

Effect of Welding Parameters on Nanostructured Fe-(C, B)-(Cr, Nb) Alloys

***Jonathan Gramajo*[a,d]*, *Agustín Gualco*[a,b], *Hernan Svoboda*[b,c]**

[a]*Universidad Nacional de Lomas de Zamora, Facultad de Ingeniería, Buenos Aires, Argentina.*
[b]*Consejo Nacional de Investigaciones Científicas y Técnicas (CONICET), Buenos Aires, Argentina.*
[c]*Universidad de Buenos Aires, Facultad de Ingeniería, Buenos Aires, Argentina.*
[d]*Comisión de Investigaciones Científicas (CIC), La Plata, Argentina.*

Received: August 15, 2019; Revised: October 22, 2019; Accepted: November 02, 2019

New nanostructured Fe-(Nb,Cr)-(C,B) multicomponent alloys have been developed for hardfacing application. They have better wear resistance than traditional Fe-Cr-C alloys. The nano-alpha-Fe, eutectic and hard carboborides phases of the weld metal usually show variations with the welding procedure. 6 test samples with different heat input were welded. It was observed that the percentage of eutectic phase and the distance between carboborides increased for the high heat input. Microhardness of eutectic phases showed a linear relationship with the spacing. Samples with high percentage of alpha-Fe phases showed a severe plastic deformation. Wear resistance was optimal for thinner eutectics phases. The presence of needles carboborides improved wear resistance.

Keywords: *Abrasion Wear; Carboborides, Hardfacing, Welding.*

1. Introduction

Abrasive wear is a phenomenon that affects a wide range of industries such as mining, cement, metal mechanical and chemical. Many components belonging to these industries such as rock or mineral drill crushers, mechanical shovels, rock grinding teeth, sludge extraction pipes, metallurgical dust conveyors and grain grinders are exposed to abrasive wear producing a loss of several millimeters [1]. The factors that determine the intensity of abrasion and affect the wear mechanisms are the type of abrasive determined by the hardness, shape and size of the abrasive particle, the operating conditions that involve the type of movement, the contact pressure and the environmental conditions of the tribosystem, and finally by the microstructure of the material that defines its mechanical properties [2-4]. Within these factors, the microstructure is a variable that controls the behavior to wear through the morphology and distribution of phases and micro-constituents formed after solidification. A clear example of this fact has been reported in the eutectic carbon steels where the thinner of the interlaminar spacing of the perlite decreases the wear rate at high pressure and sliding speed. This fact does not occur in the case of its spheroidization since the particles of cementite in a spheroidal structure show little resistance to plastic deformation causing the decrease in wear resistance compared to the laminar perlite in the same conditions [5-8]. Recently modern Fe-based nanostructured alloys resistant to abrasion wear have been designed. The selection of chemistry component should comply some of these rules: (1) multi-component consisting of more than three elements, (2) significant atomic size mismatches above 12%, and (3) negative heats of mixing [9-14]. In the processes of welding, the microstructure can be modified changing the heat input, which produced different cooling rates and as result the precipitation of phases and eutectic carbides with different morphologies. The heat input depends on current, voltage and travel speed. The amount of welding current has the greatest effect on the deposition rate and the weld penetration. The deposition rate of the process increases as the welding current increases. The travel speed influences the weld penetration and the shape of the weld deposit [15-16]. In semiautomatic welding, when the travel speed is decreased, the amount of filler metal deposited increases [15-16]. In this sense, the aim of this work was to study the effect of welding parameters in nanostructured alloys under abrasive wear.

2. Experimental

A tubular self-shielded type consumable with a diameter of 1.6 mm was used for the semi-automatic welding of 6 samples in a single stringer bead in flat position, without shielding gas protection. The stick out was 25 mm and the based metal was a low alloy steel. Six carbon steel plates (0.12%C, 0.53 %Mn, 0.14 %Si, Fe bal.) were used as base metal. A Miggytrac System was applied for moving of the torch. The travel speed was setting at 18, 30 and 42 cm/min. The welding current and voltage were detected using a digital oscilloscope.

The chemical composition was determined in the last bead by optical emission spectroscopy (OES). Boron was analyzed by plasma emission spectroscopy (PES). The different samples were identified with letters and numbers based on the electrical power and welding speed used respectively, defining two series: low (L) and high (H). The welding parameters can be seen in Table 1.

*e-mail: nahuel_jona@yahoo.com.ar

Microstructure was characterized by X-ray diffraction (XRD) on the surface of each bead. The equipment used was a RIGAKU with Cu K-α radiation between 35 ° and 95 ° with a scanning speed of 1 °/ min. The crystallite size was determined using the Scherrer equation [17]. The microstructure was analyzed by means of scanning electron microscopy (SEM) using secondary electrons (SE). Measurements of Vickers microhardness HV_2 (20 N) and on the phases with $HV_{0.05}$ (0.5 N) were made. The percentage of phases was quantified by image analysis software. The tests were conducted using a pin-on-disc machine [18]. Due to the wear test parameters are fairly arbitrary, the volumetric wear rate is not a suitable parameter for comparison with other work. However, it can be used the wear resistance relative to a reference material [19]. Low carbon steel in the annealed condition was used as the reference material. The load applied was 3 N. Three pins of 6.5 mm in diameter and 20 mm in length were extracted from the center of bead for each coupon by wire-electrical discharge machining. The surfaces of the pins were polished with diamond paste with a grain size of 3μm before each test in order to obtain surfaces free of grooves that could modify the study of the abrasion mechanisms. The tests were carried out with 150 grit silicon carbide abrasive paper. The applied load was 30 N and the sliding distance was 50 m, the speed was 20 mm/s without overlapping the pin paths. The samples were cleaned by means of ultrasound with acetone for 10 minutes before and after each test. An analytical balance was used to measure the weight loss with an accuracy of 0.0001 gr. The room temperature and humidity where the tests were carried out were 24 °C and 70 % respectively.

3. Results

Table 2 shows the result of the chemical analysis obtained on the weld metal.

The deposited material presented a high concentration of alloying elements within the Fe-(Nb, Cr)-(C,B) system. The chemical composition complies with the rules for the formation of nanostructures. These characteristics present great difficulties for the nucleation and the growth of layers of regular atoms producing crystals of nanometric size or eutectic structures [14].

Figure 1 shows the macrocuts of the different samples in which no macroscopic defects, porosities or inclusions could be seen.

The dilution percentage with the based metal varied for the different welding conditions, 38 to 35 for Low and 33 to 29 for High samples. The C, Si, Cr, Nb and B percentage increased with the increase of heat input. This would be related to the higher melting rate of material. The decrease in welding speed caused an increase in deposited metal and lower dilution [15,16].

Figure 2 are presented the X-ray diffraction patterns in two groups, L= low and H=high electrical power.

The phases identified are: α-Fe, carboborides $M_7(BC)_3$ and $M_{23}(BC)_6$ and niobium carbides NbC. The fraction of eutectic phase increased with the increase of welding speed for L group. This would be associated with the dilution. The test welded with high heat input (H3) presented the highest amount of metal carboborides. The percentage of niobium carbides were between 1 to 4 %. The crystallite size of α-Fe was between 80 and 180 nm: these variations could be related to the percentage of all precipitates, which could affect the distribution of the alloying elements [20-22] and, as a consequence, the crystallite size.

Table 1. Welding parameters

Sample	Voltage (V)	Current (A)	Electrical power [kW] = [V]*[A]	Welding speed [cm/min]	Heat input [kJ/mm]
L3	20	250	5.0	18	1.7
L5	20	250	5.0	30	1.0
L7	20	250	5.0	42	0.7
H3	35	300	10.5	18	3.5
H5	35	300	10.5	30	2.1
H7	35	300	10.5	42	1.5

Table 2. Chemical composition of the weld metal (% by weight)

Sample	Heat input [kJ/mm]	C	Mn	Si	Cr	Nb	B	Fe
L7	0.7	0.69	0.28	0.66	10.9	3.0	2.9	Bal.
L5	1.0	0.72	0.28	0.70	11.6	3.2	3.0	Bal.
L3	1.7	0.73	0.27	0.71	11.8	3.2	3.1	Bal.
H7	1.5	0.76	0.27	0.74	12.3	3.4	3.2	Bal.
H5	2.1	0.78	0.27	0.77	12.6	3.5	3.3	Bal.
H3	3.5	0.78	0.26	0.78	12.8	3.5	3.3	Bal.

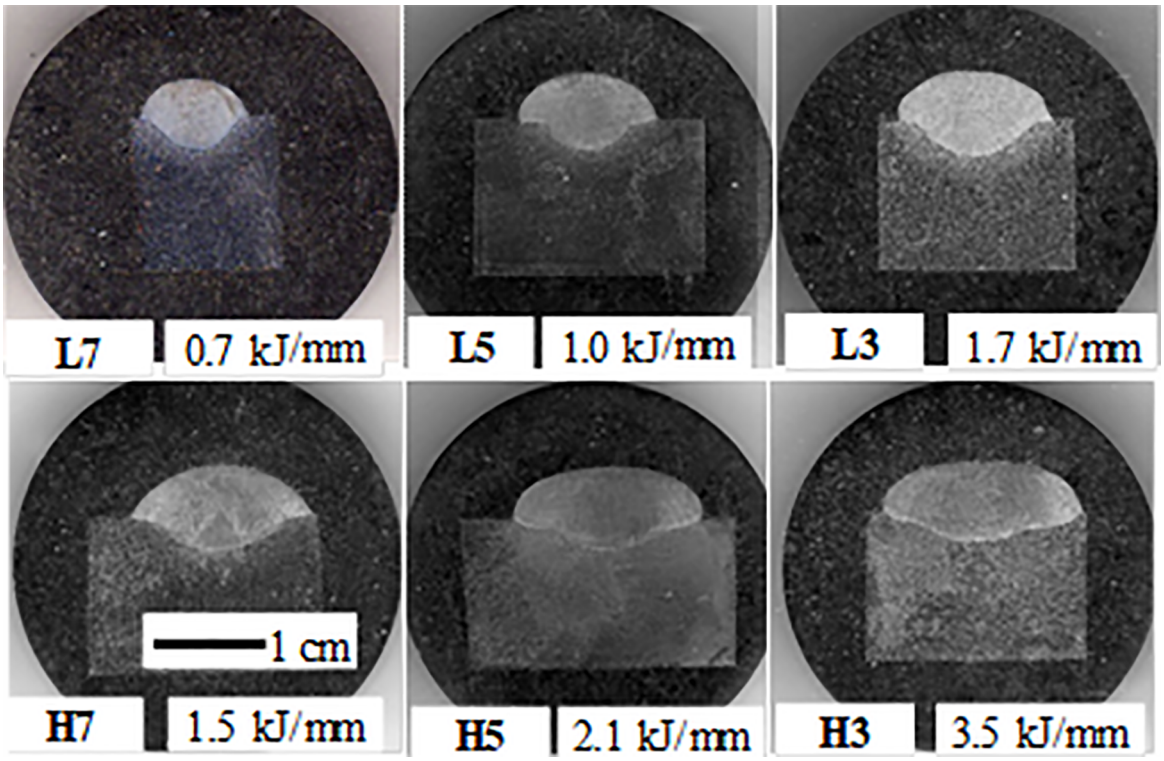

Figure 1. Transverse sections of welded coupons.

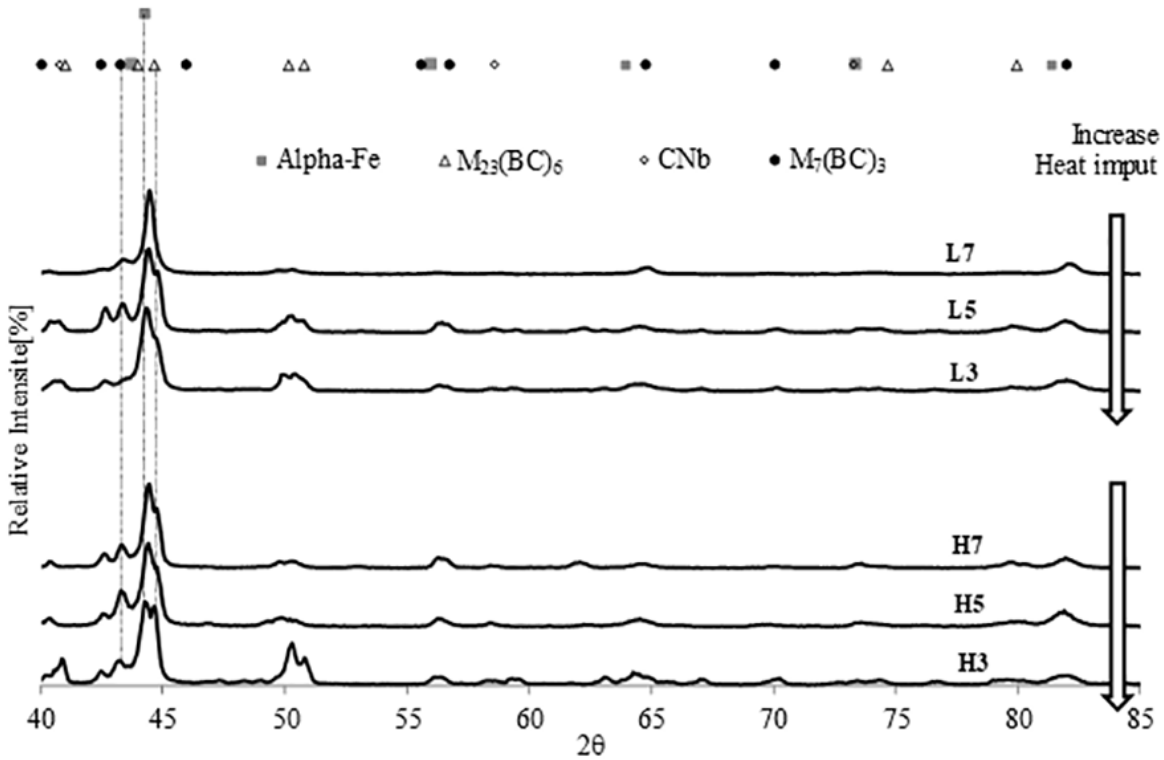

Figure 2. X-ray diffraction pattern.

Figure 3 shows the microstructures as a function of the heat input.

In relation to the samples with low heat input, the microstructure shows a dendritic segregation mode formed by α–Fe and eutectic phases. It can be seen the primary alpha irons, in L7 condition, are dendrites connect to each other, but in L5 and L3 this phase appears as a cluster or separated zones. Furthermore, in the higher heat input condition it can be seen eutectic phase with needles of $M_7(BC)_3$. The eutectic phase consisted on carboborides with the length of 10 mm and width of 2 mm (H3) which decreased in size when decreased the heat input to values of 0.5mm x 1mm (L7). In addition, the percentage of eutectic phase increased with the increased of heat input. The samples H5 and H3 showed needles carboborides, type $M_7(BC)_3$, until 20 mm of length. Both effects would be related to levels of dilution and cooling rate [23].

Figure 4 shows the percentages of phases calculated from the micrographs.

The samples welded with low heat input are formed by α–Fe + eutectic phases and those with higher heat input show the presence of elongated carboborides of M_7BC_3 + eutectic phases. This is consistent with the X-ray diffraction patterns. This would indicate two solidification modes: one dendritic and another faceted. The dendritic solidification consisted on the formation of primary α–Fe and then the segregated liquid changes into eutectic. The faceted solidification produced initial formation of needles carboborides and then the remaining liquid transformed into eutectic. It is interesting to remark that samples with high heat input had the lowest dilution and consequently the presence of phases rich in alloying elements. The niobium carbides were formed further of the solidification line in the mixing zone due to a higher melting point. Later they were trapped in the last remaining liquid that finally transformed into the eutectic phase in Figure 5. No changes were observed in the size of the carbide depending on the heat input.

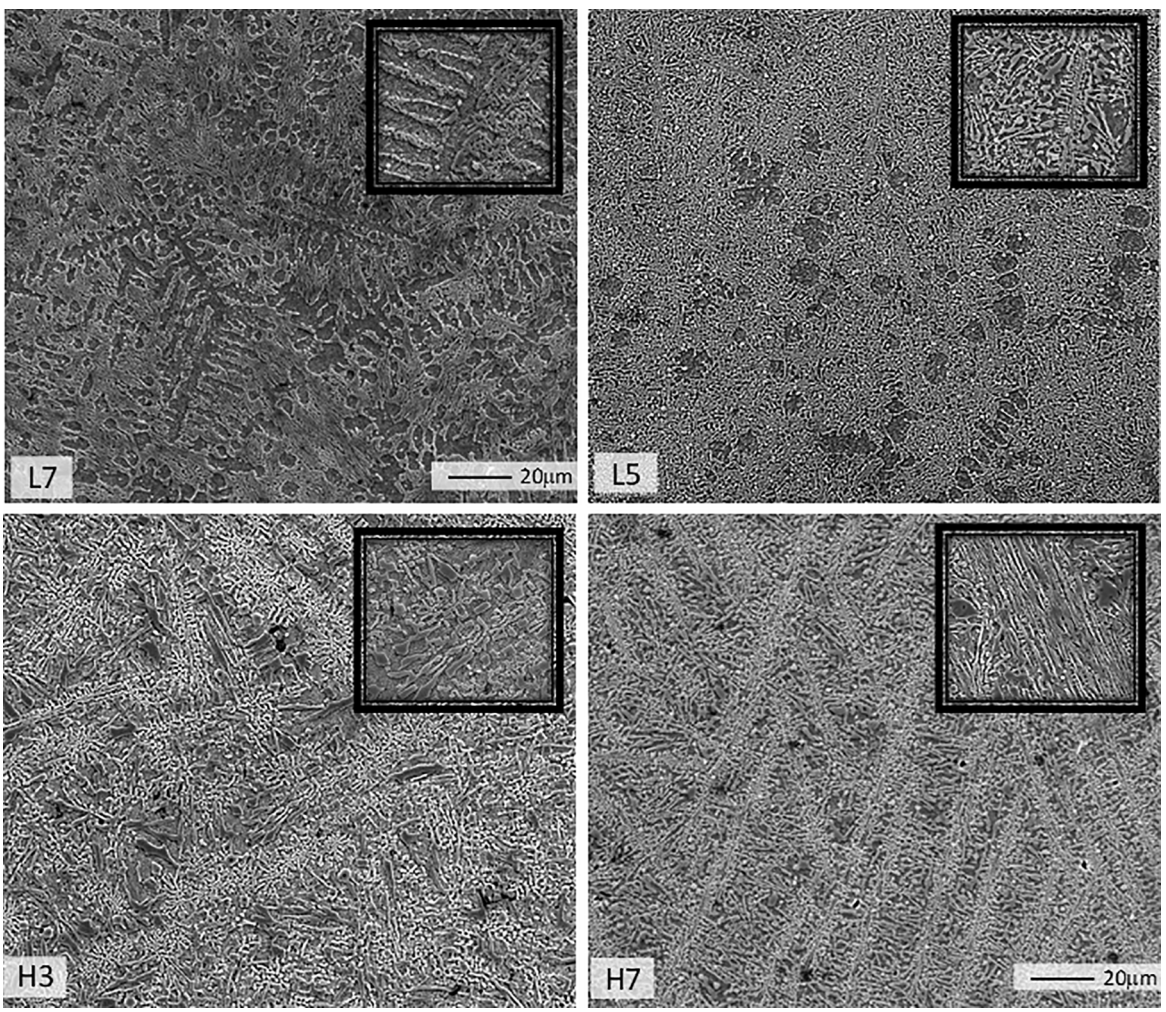

Figure 3. Microstructures of the welded samples

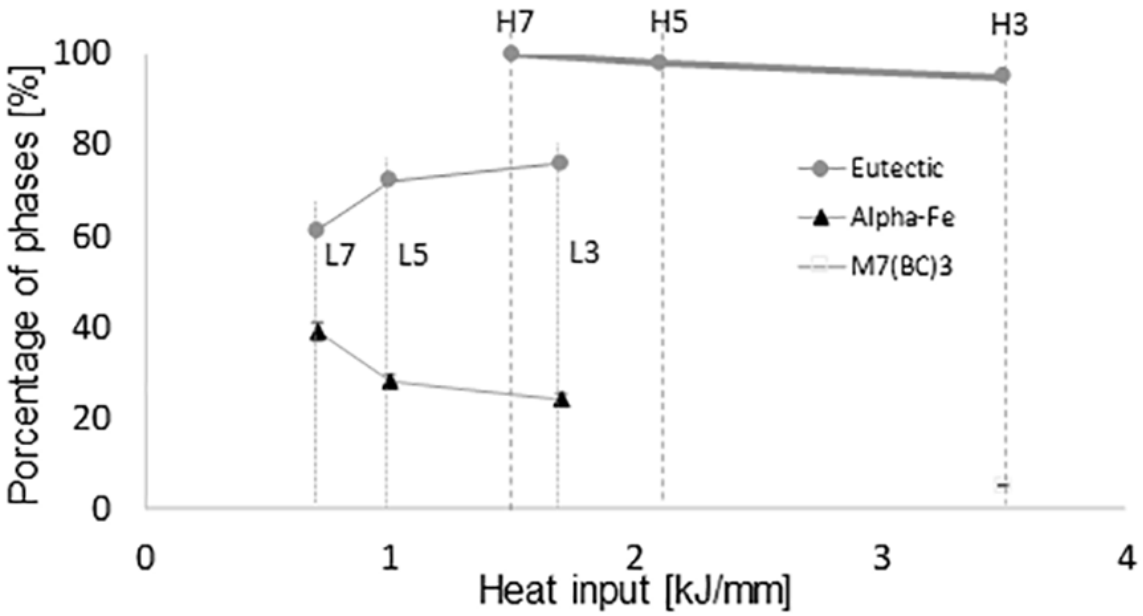

Figure 4. Phases percentages of all samples.

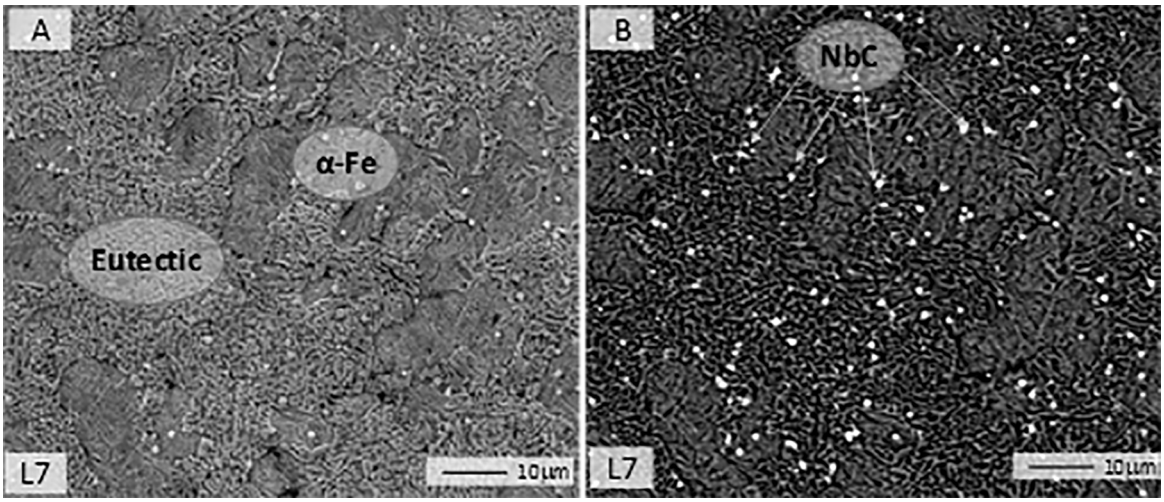

Figure 5. Images of secondary electrons (A) and backscattered electrons (B) of L7 sample.

The microhardness of the eutectic phase varied from 830 HV for H3 to 920 HV for L7. A linear relationship was observed between the heat input and the eutectic microhardness, being the highest values for the samples with lower heat input, Figure 5. This could be related to a higher cooling rate that produced finer eutectic. This reduction in distance between hard phases decreased the sliding distance for moving of dislocations performing an increase of shear stress or hardness [24-25]. The beads hardness reached maximum values for the samples welded with higher heat input (figure 6). This would be related to the presence of hard phases such as needles carboborides M_7BC_3, (about 1450 HV). The test samples welded with lower heat inputs showed a decrease in the microhardness related to the hardness of the α–Fe phase (around 540 HV).

The relative wear resistances (RW), presented linear correlation function between L5-H5 condition, as shown in Figure 7.

The eutectic phase controlled the wear abrasion and α–Fe or needles carboborides $M_{23}BC_6$ did not have influence in the wear mechanism between L5 to H5. Although in L7 condition, when the α-Fe consisted on the dendrites connected to each other, microcutting increased strongly. In H3 sample the elongated $M_{23}BC_6$ improved its wear resistance.

In Figure 8, worn surface images of the samples tested are shown.

All worn surfaces presented abrasion lines as a result of the micro-cutting wear. Figure 8a, b and c show the grooves produced by the hard particles (SiC) and severe plastic deformation at the edges which would be related to the plastic deformation effect.

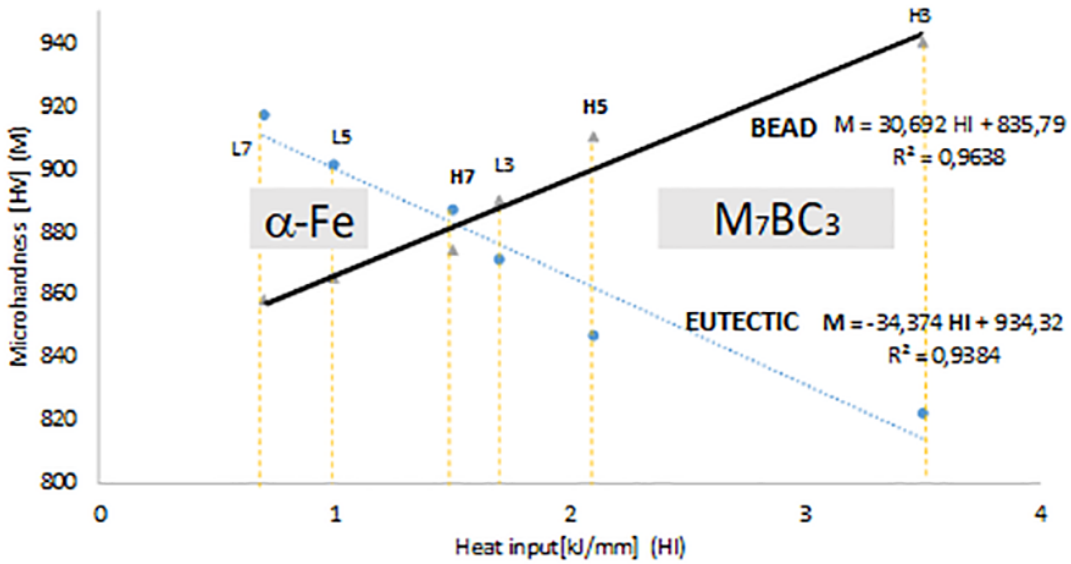

Figure 6. Relationship between microhardness and heat input.

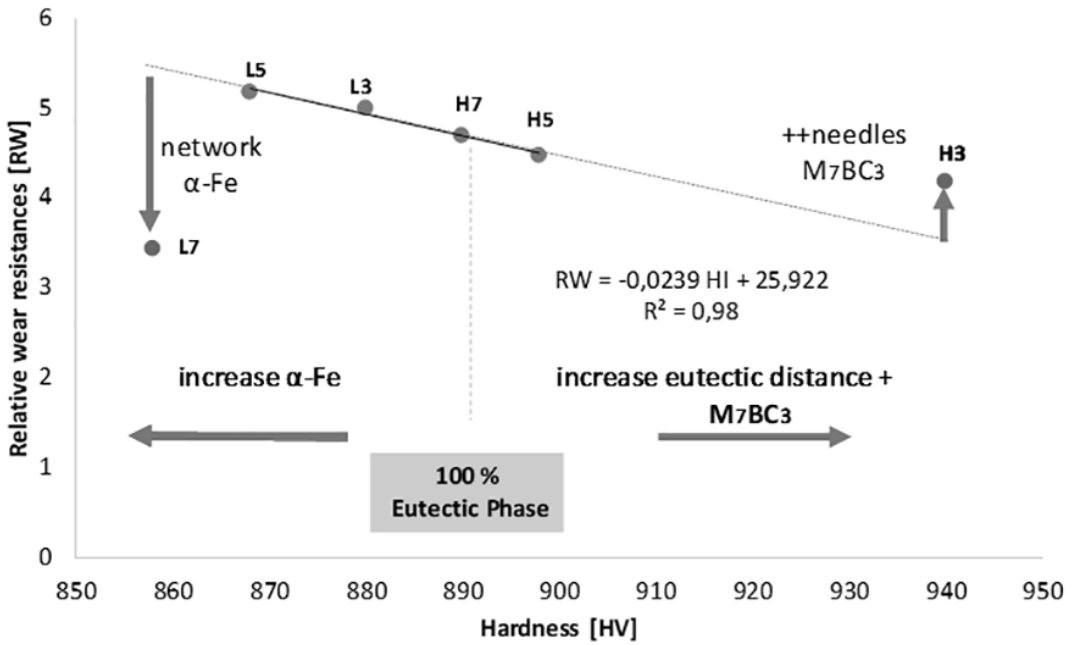

Figure 7. Weight of loss for each sample.

Microcracks were identified within the abrasion grooves as well as at the edges. They could be initiated in the interface of the eutectic carboboride [26-28]. Niobium carbides had not affected on wear resistance because their size was much smaller than the silicon carbide and they were torn off together with the matrix as shown in figures 8 a and c. In Figure 8d it can be seen how the damage on the surface had increased, the SiC penetrated being embedded in the welded material. This would be related to the higher presence of α–Fe as inter-network phase [30] indicated in figure 3.

The roughness values of Figure 9 showed a severe cutting in L7 and in L3 presented minor roughness associated with the low penetration of the hard particles. This is consistent with reported in worn surface. The samples with low heat input (L7) formed by eutectic structure with dendrites inter-network of α–Fe phased didn't shown scratch resistance producing an excessive plastic deformation and weight loss. However, when matrix consisted on eutectic carboborides with cluster of α-Fe or needles of M_7BC_3 (L3) there was observed resistance to cutting and lower ductility at the matrix-carboboride interface which produced the beginning of failure [30].

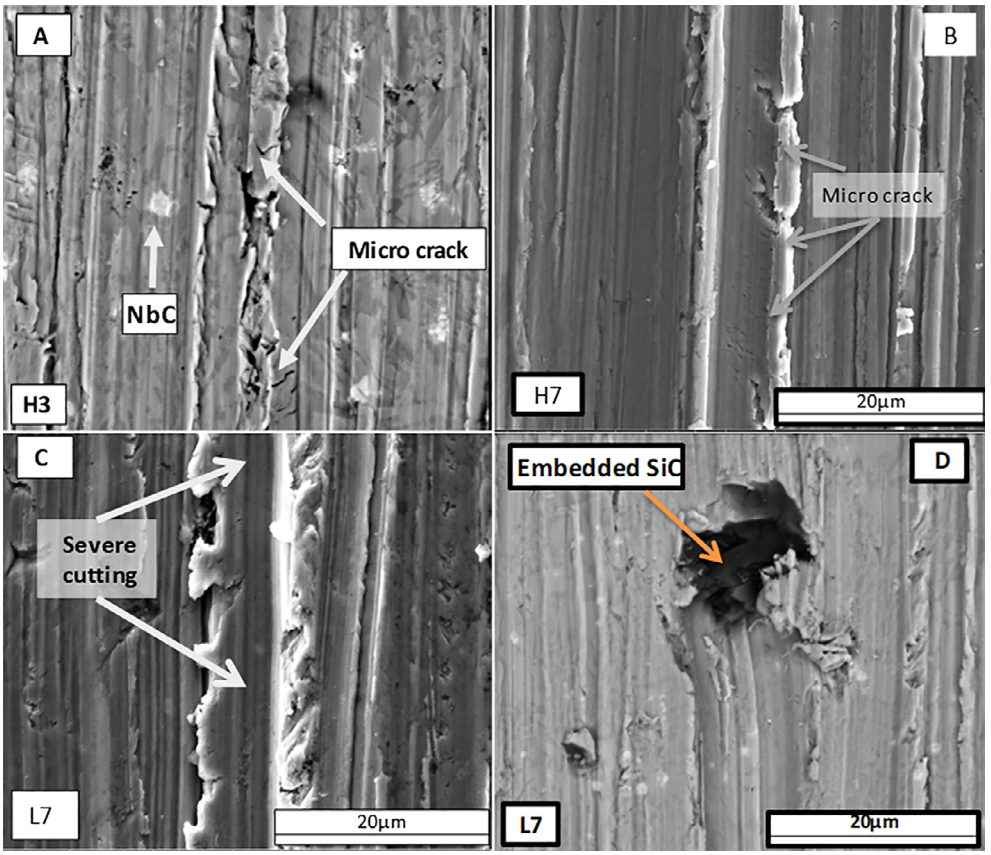

Figure 8. Worn surface images. Electron backscattered image in figure F.

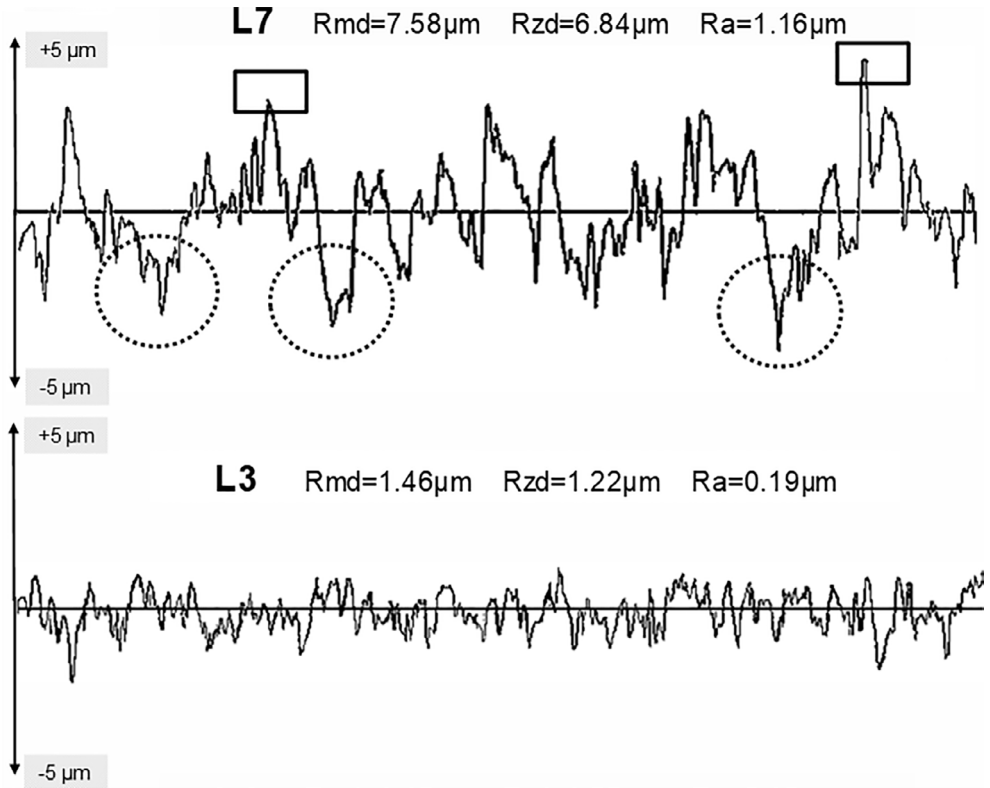

Figure 9. Roughness profiles of L7 and L3 samples.

4. Conclusions

- The deposited material presented a high concentration of alloying elements within the Fe-(Nb, Cr)-(C,B) system.

- The dilution percentage varied 38 - 29 % for L7 to H3 respectively. It could be associated which the increase of welding current and as consequence higher melting rate. The decrease in welding speed caused an increase in deposited metal.

-The microstructures were: low fraction of carboborides M_7BC_3 and eutectic phase for the samples with low dilution and α-Fe matrix with a eutectic phase ($M_{23}BC_6$ and α-Fe) for the samples with a high dilution. The eutectic phase was thinner with the increase of cooling rate.

- A linear relationship was observed between the heat input and the microhardness of eutectic phase, being the highest values for the test pieces welded with lower heat input. The hardness of α-Fe phase was around 540 HV.

- The specimens that presented the lower wear rate were those with eutectic carbide thinner. The wear mechanism was microcutting. The sample with α-Fe in network morphology presented higher plastic deformation and low abrasive wear resistance. In sample with low dilution appears needles M_7BC_3 which improve de wear resistance.

5. Acknowledgement

The authors wish to thank Eutectic-Conarco Argentina for the provision of the consumable used in this work, Air Liquide Argentina for the free supply of welding gases; Conarco-Esab Argentina for conducting chemical analyses; INTI-Electronic Microscopy Laboratory for the facilities of scanning electron microscopy.

6. References

1. Jankauskas V. Strengthening machine elements working under abrasive environment by alloying with hard layers and their estimation. *Mechanika*. 2006;57(1):55-60.

2. Pawar S, Jha AK, Mukhopadhyay G. Effect of different carbides on the wear resistance of Fe-based hardfacing alloys. *International Journal of Refractory Metals and Hard Materials*. 2019;78:288-295.

3. De Pelegrin DV, Stachowiack GW. Assessing the role of particle shape and scale in abrasion using 'sharpness analysis': Part II. Technique evaluation. *Wear*. 2002;253(9-10):1026-1034.

4. Xie Y, Bhushan B. Effects of particle size, polishing pad and contact pressure in free abrasive polishing. *Wear*. 1996;200(1-2):281-295.

5. Wang Y, Pan L, Lei T. Sliding wear of pearlitic structures in eutectoid steel. *Wear*. 1991;143(1):57-69.

6. Larsen-Badse J, Mathew KG. Influence of structure on the abrasion resistance of 1040-steel. *Wear*. 1969;14(3):199-205.

7. Buchely MF, Gutierrez JC, León LM, Toro A. The effect of microstructure on abrasive wear of hardfacing alloys. *Wear*. 2005;259(1-6):52-61.

8. Gahr KHZ. *Microstructure and Wear of Materials. Tribology Series*. Volume 10. Amsterdam: Elsevier; 1987.

9. Heath G. Nanotechnology and Welding – Actual and possible future applications. In: *Proceedings of the Castolin-Eutectic Seminar*; 2006 Oct 25; Brussels: Belgium. p. 25-35.

10. Branagan DJ. Engineering structures to achieve targeted properties in steels on a nanoscale level. *Calphad*. 2007;31(3):343-350.

11. Kirchgaßner M, Badish E, Franek F. Behaviour of iron-based hardfacing alloys under abrasion and impact. *Wear*. 2008;265(5-6):772-779.

12. Branagan DJ, Marshall MC, Meacham BE. High toughness high hardness iron based PTAW weld materials. *Materials Science and Engineering: A*. 2006;428(1-2):116-123.

13. Bahoosh M, Shahverdi RH, Farnia A. Macro-indentation fracture mechanisms in a super-hard hardfacing Fe-based electrode. *Engineering Failure Analysis*. 2018;92:480-494.

14. Inoue A. Stabilization of metallic supercooled liquid and bulk amorphous alloys. *Acta Materialia*. 2000;48(1):279-306.

15. Norrish J. *Advanced Welding Processes*. Oxford: Woodhead Publishing; 2006.

16. Hobart Institute of Welding Technology. *Flux Cored Arc Welding*. Troy: Hobart Institute of Welding Technology; 2012.

17. Cullity BD, Stock SR. *Elements of X-ray Diffraction*. 3rd ed. New York: Prentice Hall; 2001. 520 p.

18. ASTM International. *ASTM G132-96 (2018) - Standard Test Method for Pin Abrasion Testing*. West Conshohocken: ASTM International; 2018.

19. Moore MA. The relationship between the abrasive wear resistance, hardness and microstructure of ferritic materials. *Wear*. 1974;28(1):59-68.

20. Gleiter H. Nanostructured materials: basic concepts and microstructure. *Acta Materialia*. 2000;48(1):1-29.

21. Weissmüller J. Alloy effects in nanostructures. *Nanostructured Materials*. 1993;3(1-6):261-272.

22. Inoue A, Hashimoto K. *Amorphous and nanocrystalline materials: Preparation, Properties, and Applications*. Berlin, Heidelberg: Springer; 2010. 206 p.

23. Gualco A, Svoboda HG, Surian ES. Study of abrasive wear resistance of Fe-based nanostructured hardfacing. *Wear*. 2016;360-361:14-20.

24. Ray KK, Mondal D. The effect of interlamellar spacing on strength of pearlite in annealed eutectoid and hypoeutectoid plain carbon steels. *Acta Metallurgica et Materialia*. 1991;39(10):2201-2208.

25. Xu L, Kennon NF. A study of the abrasive wear of carbon steels. *Wear*. 1991;148(1):101-112.

26. De Pellegrin DV, Torrance AA, Haran E. Wear mechanisms and scale effects in two-body abrasion. *Wear*. 2009;266(1-2):13-20.

27. Chattopadhyay R. *Surface Wear: Analysis, Treatment, and Prevention*. Materials Park: ASM International; 2001.

28. Çimenoğlu H. Subsurface characteristics of an abraded low carbon steel. *Wear*. 1997;210(1-2):204-210.

29. Lai HH, Hsieh CC, Lin CM, Wu W. Effect of oscillating traverse welding on microstructure evolution and characteristic of hypoeutectic hardfacing alloy. *Surface and Coatings Technology*. 2014;239:233-239.

30. Narayanaswamy B, Hodgson P, Beladi H. Comparisons of the two-body abrasive wear behavior of four different ferrous microstructures with similar hardness levels. *Wear*. 2016;350-351:155-165.